Subband Independent Component Analysis for Coherence Enhancement

Guo, Z., Xu, Y., Rosenzweig, J., McClelland, V., Rosenzweig, I. & Cvetkovic, Z.

Original citation & hyperlink:
Guo, Z, Xu, Y, Rosenzweig, J, McClelland, V, Rosenzweig, I & Cvetkovic, Z 2024, 'Subband Independent Component Analysis for Coherence Enhancement', IEEE Transactions on Biomedical Engineering, vol. (In-Press), pp. (In-Press).
https://dx.doi.org/10.1109/TBME.2024.3370638

DOI 10.1109/TBME.2024.3370638
ISSN 0018-9294
ESSN 1558-2531

Publisher: Institute of Electrical and Electronics Engineers (IEEE)

Subband Independent Component Analysis for Coherence Enhancement

Zhenghao Guo, Yuhang Xu, Jan Rosenzweig, Verity M. McClelland, Ivana Rosenzweig, and Zoran Cvetkovic

***Abstract*—*Objective:* Cortico-muscular coherence (CMC) is becoming a common technique for detection and characterization of functional coupling between the motor cortex and muscle activity. It is typically evaluated between surface electromyogram (sEMG) and electroencephalogram (EEG) signals collected synchronously during controlled movement tasks. However, the presence of noise and activities unrelated to observed motor tasks in sEMG and EEG results in low CMC levels, which often makes functional coupling difficult to detect. *Methods:* In this paper, we introduce Coherent Subband Independent Component Analysis (CoSICA) to enhance synchronous cortico-muscular components in mixtures captured by sEMG and EEG. The methodology relies on filter bank processing to decompose sEMG and EEG signals into frequency bands. Then, it applies independent component analysis along with a component selection algorithm for re-synthesis of sEMG and EEG designed to maximize CMC levels. *Results:* We demonstrate the effectiveness of the proposed method in increasing CMC levels across different signal-to-noise ratios first using simulated data. Using neurophysiological data, we then illustrate that CoSICA processing achieves a pronounced enhancement of original CMC. *Conclusion:* Our findings suggest that the proposed technique provides an effective framework for improving coherence detection. *Significance:* The proposed methodologies will eventually contribute to understanding of movement control and has high potential for translation into clinical practice.**

***Index Terms*—Cortico-muscular coherence, filter banks, independent component analysis.**

I. Introduction

UNRAVELLING the interactions between cortical sensorimotor activity and muscle is key to understanding the underlying physiology and exploring more individualized therapies for people suffering from movement disorders. The mechanisms of cortico-muscular interactions can be studied by analysing electroencephalogram (EEG) and electromyogram (EMG) signals which are recorded synchronously from the sensorimotor cortex and muscle, respectively, during controlled movement tasks. The advantages of such neurophysiological techniques are that they are resource efficient, non-invasive and most critically offer the required time-resolution which cannot be achieved by imaging techniques. In this context, cortico-muscular coherence (CMC) analysis, which detects the presence of synchronous components in electrophysiological recordings from the brain and concurrently active muscles, is one of the most commonly used methods [2], [3], [4].

Coherence between EEG and EMG has enhanced our understanding of normal sensorimotor control [5], [6] and of the pathophysiology of movement disorders, such as tremor [6], [7], [8], myoclonus [8], [9], [10], Parkinson's disease [11], [12], [13], and dystonia [14], [15], [16]. Clinical application of EEG-EMG coherence includes distinguishing between different types of movement disorder, such as tremor versus myoclonus [8], or between different tremor types [8], [17]. However, the full potential of EEG-EMG coherence in the clinical assessment of motor disorders is yet to be fully realised, partly due to its considerable variability between individuals. Indeed, some individuals with good motor skills do not express CMC above the significance level [18], [19], [20], [21].

There are several factors that contribute to this variability and tend to lower the calculated values of CMC. One of the main reasons for the typically low level of coherence between surface EMG (sEMG) and EEG is the presence of noise and sEMG and EEG components unrelated to the task of interest, which we will refer collectively as *noise* [1]. For example, sEMG is usually recorded by electrodes placed on the skin overlying the muscle, so it can be contaminated by various types of noise, such as electrical noise from power lines and external sources, motion artefact, as well as cross-talk from other muscles [22], [23], [24]. Similarly, the scalp EEG recordings are a mixture of brain, artefactual, and other unknown random signals, *e.g.* instrumentation noise and external electromagnetic activities [25]. Even genuine physiological signals from the brain are effectively "noise" in this context, as not all brain activities recorded are relevant to the communication between cortex and muscle. When the EEG and sEMG signals are recorded, all these additional components are present within the recorded signal. Standard coherence analysis does not include steps to distinguish these different "noise components" from the signal of interest, so they are inevitably incorporated into the analysis and impact on the coherence value. The objective of this work is to develop a denoising method that is capable of enhancing the

This work was presented in part at EMBC 2017 [1].

Zhenghao Guo is with the School of Biomedical Engineering, Dalian University of Technology, Ganjingzi District, Dalian 116024, China and the Department of Engineering, King's College London, The Strand, London WC2R 2LS, UK (e-mail: zhenghaoguo@dlut.edu.cn; zhenghao.guo@kcl.ac.uk)

Jan Rosenzweig and Zoran Cvetkovic are with the Department of Engineering, King's College London, The Strand, London WC2R 2LS, UK (e-mail: {jan.1.rosenzweig; zoran.cvetkovic}@kcl.ac.uk)

Yuhang Xu is with the Research Centre for Intelligent Healthcare, Coventry University, Coventry CV1 5FB, UK (e-mail: yuhang.xu@coventry.ac.uk)

Ivana Rosenzweig is with the Department of Neuroimaging, Institute of Psychiatry, Psychology and Neuroscience, King's College London, Denmark Hill, London SE5 8AF, UK (email:ivana.1.rosenzweig@kcl.ac.uk)

Verity M. McClelland is with the Department of Clinical Neuroscience, Institute of Psychiatry, Psychology and Neuroscience, King's College London, Denmark Hill, London SE5 9RX, UK (email:verity.mcclelland@kcl.ac.uk)

coherence levels degraded by a considerable amount of noise and interference activities involved in both EEG and sEMG signals.

One approach towards eliminating noise in biological signals is based on wavelet transform thresholding [26], [27], [28], especially effective for the removal of white Gaussian noise (WGN). However, when dealing with suppressing the components with respect to the activity unrelated to the considered task, wavelet thresholding algorithms may lose their efficiency. Another algorithm that is very successful for noise reduction of multichannel biological signals is independent component analysis (ICA) [29], [30], [31], [32]. ICA, however, requires data from a sufficiently large number of channels to be able to separate independent sources, which may not be available in practice [33]. Moreover, although ICA is typically very effective for isolating artefacts, it is less effective for separating different physiological activities [34].

To overcome the limitations of the wavelet threshold denoising (WTD) and ICA, a further method was proposed, based on the joint use of wavelet decomposition and ICA, that builds on the advantages of both techniques [35]. This technique, referred to as Wavelet Independent Component Analysis (W-ICA), proved to be very effective in artefact rejection from biological signals [36], [37], [38], [39], [40], [41], [42]. Drawing inspiration from W-ICA, we develop a methodology for enhancing relative levels of components involved in *information transmission between two processes*. Whilst in this study we focus on EEG and sEMG signals and their coupling involved in movement control, the proposed methodology is more general. We propose to first generalise W-ICA to employ also subband decompositions other than the wavelet transform, and thus further increase the number of input components and exploit different frequency resolutions. In that direction, we consider subband decompositions obtained via cosine-modulated filter banks (CMFB) [43]. We provide the rationale behind the proposed methodology by postulating that in the context of ICA of neurophysiological signals, subband decompositions produce relatively fewer independent components relative to the number of mixtures, and thus facilitate their separation. Further, towards extracting components which are involved in interactions between two processes, we propose to use the subband-based ICA in combination with an automatic component selection algorithm that maximizes their coherence levels. We refer to this technique as *Coherent Subband Independent Component Analysis* (CoSICA). The proposed method is designed to be applied to low-channel count sEMG and EEG signals, with the aim of simplifying the operation of diagnostic data collection.

This paper is organized as follows. In Section II, relevant aspects of CMC analysis are reviewed. In Section III, we introduce the CoSICA methodology. Section IV and Section V present results of assessments of CoSICA in terms of its effectiveness for increasing CMC, using both simulated data under different signal-to-noise ratios (SNRs) and neurophysiological data, respectively. Finally, the results are discussed in Section VI and conclusions are drawn in Section VII.

II. Background

A. CMC between noisy EEG and EMG

Muscle movement is controlled by a cortical excitation signal $x_c(t)$, which is transmitted via N_x paths; each path may have a different delay D_i and attenuation b_i. The control signal received by the muscle, $y_c(t)$, together with noise $n_y(t)$, forms the corresponding sEMG signal $y(t)$. The sEMG signal thus has the form

$$y(t) = y_c(t) + n_y(t) = \sum_{i=1}^{N_x} b_i x_c(t - D_i) + n_y(t) \ , \qquad (1)$$

where $n_y(t)$ is a combination of noise in a general sense and various other events unrelated to the considered task. Analogously, a synchronously recorded EEG signal $x(t)$ is a mixture of muscle-control activity $x_c(t)$ and a component $n_x(t)$ that is a combination of artefacts, other cortical events, and noise. Therefore, the EEG signal has the form $x(t) = x_c(t) + n_x(t)$.

Cortico-muscular coupling is commonly detected and quantified by means of coherence analysis [44]. The coherence $C_{xy}(\omega)$ between two stationary processes $x(t)$ and $y(t)$ is defined as

$$C_{xy}(\omega) = \frac{|S_{xy}(\omega)|^2}{S_{xx}(\omega) S_{yy}(\omega)} \ , \qquad (2)$$

where $S_{xx}(\omega)$ and $S_{yy}(\omega)$ are their power spectral densities, and $S_{xy}(\omega)$ is their cross spectral density. The value of coherence is a real number between 0 and 1, with 0 indicating a complete absence of linear association between two processes such that they are totally incoherent and 1 indicating a perfect linear association such that two processes are completely coherent.

When $y_c(t)$ is the response to $x_c(t)$ via a linear time-invariant system and both $n_x(t)$ and $n_y(t)$ are independent zero-mean processes, the coherence between the sEMG and EEG signals at a frequency ω can be shown to have the form

$$C_{xy}(\omega) = \frac{|B(\omega)|^2 S^2_{x_c x_c}(\omega)}{\left(S_{x_c x_c}(\omega) + S_{n_x n_x}(\omega)\right)\left(|B(\omega)|^2 S_{x_c x_c}(\omega) + S_{n_y n_y}(\omega)\right)} \ , \qquad (3)$$

where $S_{x_c x_c}(\omega)$, $S_{n_x n_x}(\omega)$, $S_{n_y n_y}(\omega)$ are power spectral densities of $x_c(t)$, $n_x(t)$ and $n_y(t)$, and $B(\omega)$ is the frequency response of the propagation channel (1) [45]. It can be observed that, in the absence of the noise components $n_x(t)$ and $n_y(t)$, the coherence is equal to one. On the other hand, the coherence can be very low if the components $x_c(t)$ and $y_c(t)$, are weak when compared to the noise.

B. Time-frequency Representation of Coherence

In coherence analysis of non-stationary processes, spectral densities are estimated within time segments over which their statistical properties remain approximately constant. To that end, the short-time Fourier transform (STFT) is employed. Given a signal $x(t)$, its STFT within intervals centred around time instants $t_c = n\Delta t, \ n \in \mathbb{Z}$ is computed as $X(t_c, \omega) = \sum_{t=-\infty}^{\infty} x(t) w(t - t_c) e^{-j\omega t}$, where $w(t)$ is a window function designed according to time-frequency resolution requirements

and Δt is the window shift [46]. The time varying power spectral and cross-spectral densities are estimated by averaging the STFT magnitude spectra over different epochs (trials): $\hat{S}_{xx}(t_c,\omega) = \frac{1}{L}\sum_{n=1}^{L}|X_n(t_c,\omega)|^2$, and analogously for $\hat{S}_{yy}(t_c,\omega)$, while $\hat{S}_{xy}(t_c,\omega) = \frac{1}{L}\sum_{n=1}^{L}X_n(t_c,\omega)Y_n^*(t_c,\omega)$, where * denotes the complex conjugate, L is the number of epochs, and $X_n(t_c,\omega)$ and $Y_n(t_c,\omega)$ are the short-time Fourier transforms of the nth trial of $x(t)$ and $y(t)$. Therefore, the coherence between $x(t)$ and $y(t)$ is computed as

$$C_{xy}(t_c,\omega) = \frac{|\hat{S}_{xy}(t_c,\omega)|^2}{\hat{S}_{xx}(t_c,\omega)\hat{S}_{yy}(t_c,\omega)} \ . \tag{4}$$

Significant coherence can be defined by setting the confidence limit (CL) to 95% which is estimated as

$$\mathrm{CL}_{(a\%)} = 1 - \left(1 - \frac{\alpha}{100}\right)^{\frac{1}{(L-1)}} \ , \tag{5}$$

where α is set to 95 [47].

III. Coherent Subband Independent Component Analysis

A. Subband Decompositions

Consider a set of signals $y_m(t),\ m = 1,...,M$ which are mixtures of components $c_i(t),\ i = 1,\dots I$, that is

$$y_m(t) = \sum_{i=1}^{I}\alpha_{mi}c_i(t) \ .$$

In a situation where there are fewer mixtures than components, $M < I$, in general it may not be possible to identify the independent components. If we filter the mixtures with J filters $h_j(t),\ j = 1,\dots J$, we obtain J times as many mixtures[1]

$$y_{m,j}(t) = y_m(t) * h_j(t) = \sum_{i=1}^{I}\alpha_{mi}c_i(t) * h_j(t) \ ,$$

but that does not necessarily provide an advantage, since in general the number of components is increased by the same factor, *i.e.* every component $c_i(t)$ gives rise to J components $c_i(t) * h_j(t),\ j = 1,\dots J$, and they are no longer statistically independent. If, on the other hand, a substantial set of the filtered independent components are equal to zero, $h_j(t) * c_i(t) = 0$, the ratio between the number of mixtures and the number of components increases. Thus, if based on domain specific knowledge, filters h_i are designed so that each filter removes one or more independent components, then the effective number of mixtures will increase relative to the number of components. In motor control, different frequency bands have different functional importance, which suggests that subband-based ICA could be particularly effective in the context of separating independent components from low-channel count sEMG and EEG recordings. In this study, we propose using dyadic stationary wavelet transform (SWT) and CMFB for subband decomposition so as to obtain different frequency resolutions. The details are in the following.

[1]We use $*$ to denote the convolution operator,

$$c(t) * h(t) = \sum_{\tau=-\infty}^{\infty} c(\tau)h(t-\tau) \ .$$

1) Dyadic stationary wavelet transform: The dyadic SWT used in this study decomposes the M mixture signals with wavelet filters across $J-1$ scales into MJ filtered mixture signals $y_{m,j}(t),\ j = 1,...,J$. These are obtained by convolving y_m using filters $h_{J-1,0}(t)$ and $h_{j,1}(t),\ j = 1,...,J-1$, as

$$y_{m,j}(t) = \begin{cases} h_{J-1,0}(t) * y_m(t) \ , & j = J \ , \\ h_{j,1}(t) * y_m(t) \ , & j = 1,\dots,J-1 \ . \end{cases} \tag{6}$$

The filters are derived from two prototype filters $h_0(t)$ and $h_1(t)$ through an iterative procedure that is specified in the z-transform domain as

$$H_{J-1,0}(z) = \prod_{k=0}^{J-2} H_0(z^{2^k}) \ ,$$
$$H_{j,1}(z) = H_1(z^{2^{j-1}})\prod_{k=0}^{j-2} H_0(z^{2^k}) \ .$$

The prototype filters $h_0(t)$ and $h_1(t)$ are designed to be half-band low-pass and half-band high-pass, respectively. Hence, $y_{m,j}(t),\ j = 1,\dots,J$ are components of $y_m(t)$ occupying approximately frequency bands

$$\left(\frac{f_s}{2^{j+1}}, \frac{f_s}{2^j}\right), j = 1,\dots J-1, \text{ and } \left(0, \frac{f_s}{2^J}\right) \ ,$$

respectively, where f_s is the sampling frequency [48]. If signals are acquired using sampling frequency $f_s = 1024$ Hz, and the wavelet transform is computed at $J-1 = 7$ scales, then $y_{m,3}(t)$, $y_{m,4}(t)$, $y_{m,5}(t)$, $y_{m,6}(t)$, $y_{m,7}(t)$ and $y_{m,8}(t)$ occupy approximately high γ $(64-128)$ Hz, low γ $(32-64)$ Hz, β $(16-32)$ Hz, α $(8-16)$ Hz, θ $(4-8)$ Hz, and δ $(0-4)$ Hz bands of neural oscillations, respectively. Increasing the number of scales of the wavelet transform divides recursively only the lowest band in two, whereas all other bands remain unchanged, as evident from the filter structure.

A signal $y_m(t)$ can be reconstructed from its wavelet components according to

$$\begin{aligned} y_m(t) =& \frac{1}{2^{J-1}}\tilde{h}_{J-1,0}(t) * y_{m,J}(t) \\ &+ \sum_{j=1}^{J-1}\frac{1}{2^j}\tilde{h}_{j,1}(t) * y_{m,j}(t) \ , \end{aligned} \tag{7}$$

where the superscript $\tilde{}$ indicates time reversal. Figures 1(a) and 1(b) illustrate an analysis-synthesis filter bank for a 3-scale SWT. Note that compared to the conventional discrete wavelet transform (DWT), the downsampling operators are removed from the channels [49], which allows for translation-invariance and retains the same amount of samples in each subband for ICA.

2) Cosine-modulated filter bank: Towards exploring an alternative subband decomposition, with the potential for an increased number of components and finer frequency resolution at high frequencies, we propose using the CMFB. Figure 2 illustrates a J-channel maximally decimated filter bank. For each input $y_m(t)$, the analysis filters $f_j(t),\ j = 1,...,J$ decompose it into J subband signals that are then decimated by J, according to

$$y_{m,j}(t) = \sum_{\tau=-\infty}^{\infty} f_j(\tau)y_m(Jt-\tau) \ . \tag{8}$$

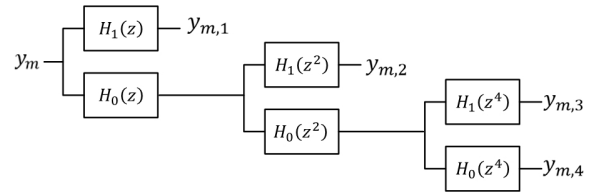

(a) SWT analysis filter bank.

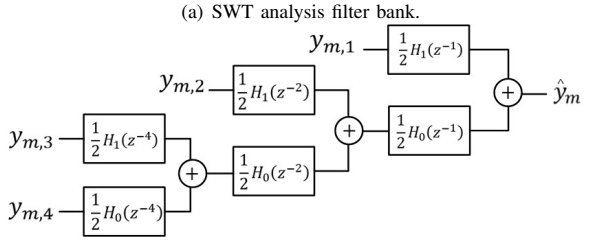

(b) SWT synthesis filter bank.

Fig. 1. An illustration of a 3-level SWT decomposition and reconstruction filter bank, where $J = 4$.

The signal $y_m(t)$ can be reconstructed from its subband components as

$$y_m(t) = \sum_{j=1}^{J} \sum_{\tau=-\infty}^{\infty} g_j(t - J\tau) y_{m,j}(\tau) \ , \tag{9}$$

where $g_j(t)$ are the synthesis filters following the interpolators. Analogously to the SWT (or the non-decimated DWT), we considered also CMFB decompositions without the decimation in the channels. Our empirical results showed however, that the proposed CoSICA achieves better results with the decimation.

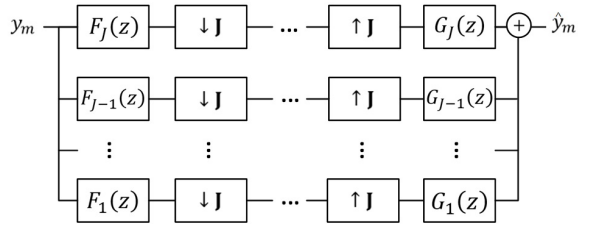

Fig. 2. An illustration of a J-channel maximally decimated filter bank.

The filters $f_j(t)$ and $g_j(t)$ can be obtained by cosine-modulation of a prototype filter $f(t)$

$$f_j(t) = 2f(t)\cos\left((2j-1)\left(\frac{\pi}{2J}\right)\left(t - \frac{L-1}{2}\right) - (-1)^j \frac{\pi}{4}\right) \ ,$$

$$g_j(t) = 2f(t)\cos\left((2j-1)\left(\frac{\pi}{2J}\right)\left(t - \frac{L-1}{2}\right) + (-1)^j \frac{\pi}{4}\right) \ ,$$

where $0 \leq t \leq L-1$, and L is the length of $f(t)$. In this study, the prototype filter design proposed in [50] is used, with filter length that is two times the number of channels, $L = 2J$.

The prototype filter $f(t)$ is designed to be a low-pass filter with a cut-off frequency of $\pi/2J$, so owing to this particular filter bank constructions, subband components $y_{m,j}(t),\ j = 1, \ldots, J$ of $y_m(t)$ occupy uniformly distributed frequency bands

$$\left(\frac{j-1}{2J} f_s, \frac{j}{2J} f_s\right), j = 1, \ldots J \ ,$$

respectively [48]. In order to extract β band $(16 - 32)$ Hz oscillations, which are involved in motor control, at sampling frequency of $f_s = 1024$ Hz, we need a CMFB with at least 32 channels. Increasing the number of channels to 64 and 128 extracts further the α, and then θ and δ bands, respectively, and divides the β band into narrower subband components.

B. Independent Component Analysis

Consider the matrix of filtered mixtures

$$\begin{aligned}\mathbf{y}(t) &= [y_{1,1}(t), ..., y_{1,J}(t), ..., y_{M,1}(t), ..., y_{M,J}(t)]^{\mathrm{T}} \\ &= [y_1(t), y_2(t), ..., y_{N_y}(t)]^{\mathrm{T}} \ ,\end{aligned}$$

where each $y_{m,j}(t),\ 1 \leq m \leq M,\ 1 \leq j \leq J$, is represented as a column vector, $y_{(m-1)J+j}(t) = y_{m,j}(t)$ and $N_y = MJ$. Let further $q_n(t),\ n = 1, \ldots, N_q$ be the independent source signals mixed according to

$$y_i(t) = \sum_{j=1}^{N_q} a_{i,j} q_j(t) \ ,$$

where $a_{i,j}$ is the (i,j) entry of the mixing matrix $\mathbf{A}$. ICA amounts to finding an estimate $\hat{\mathbf{W}}$ of the inverse matrix $\mathbf{W} = \mathbf{A}^{-1}$ by making the de-mixed components, in particular, column vectors of the matrix

$$\hat{\mathbf{q}}(t) = [\hat{q}_1(t), \hat{q}_2(t), ..., \hat{q}_{N_s}(t)]^{\mathrm{T}} \ ,$$

where

$$\hat{\mathbf{q}}(t) = \hat{\mathbf{W}}\mathbf{y}(t) \ , \tag{10}$$

maximally independent. We refer to signals $\hat{q}_i(t)$ obtained in this manner as subband independent components (SICs).

C. Subband Independent Components Selection

The problem that needs to be resolved once SICs are obtained is to find those which constitute the sought sEMG/EEG activity. In the context of CMC analysis, we propose to select SICs based on their impact on CMC levels, as those which are involved in the considered motor task should increase the overall coherence level, whereas those which are unrelated to the task should effectively act as noise that lowers the coherence. For that purpose a greedy selection algorithm is proposed. A subset of components $\hat{q}_i(t)$ selected in this manner is recombined, aiming to reconstruct a version of sEMG and EEG containing a relatively higher level of components involved in cortico-muscular coupling. The details of the proposed algorithm are as follows:

1) **Initialization.** Perform W-ICA or CMFB-ICA on sEMG signals to obtain SICs $\hat{q}_i(t),\ i = 1, 2, ..., N_s$ as input for component selection. A subband independent component (SIC) counter g is set to $g = 1$, and the initial value of CMC, C^0_{xy}, is computed as the value of CMC between EEG and sEMG that is reconstructed with all SICs.
2) **SIC removal.** The g-th SIC is removed, *i.e.* the matrix of SICs is updated with the g-th SIC set to zero, and the sEMG signal is reconstructed with the updated matrix of SICs.
3) **CMC estimation and SIC selection.** The CMC between EEG and reconstructed sEMG signals is calculated. If it is higher than C^{g-1}_{xy}, the coherence C^g_{xy} to be compared

next time will be updated with the value of CMC calculated between EEG and the reconstructed sEMG signals. Otherwise, if the CMC is lower than or equal to C_{xy}^{g-1}, the gth SIC, $q_g(t)$, is restored in the updated matrix of SICs and the reference coherence level is set to $C_{xy}^{g} = C_{xy}^{g-1}$.

4) **Iteration.** The index g is incremented by 1 and steps 2) to 3) are repeated until all SICs have been considered.
5) **Repeat.** Repeat steps 1) to 4) using reconstructed sEMG and SICs of EEG as input.

In this study, the β band CMC is taken into account during the process of the proposed component selection algorithm, since it has been found to be task dependent [3], related to motor performance [51], and modulated by different types and intensities of afferent stimuli [19]. Both the average coherence in the β band and its value at 24 Hz, the centre of the band, were used for this purpose, but the conclusions and qualitative observations remained the same. We will refer to this coherence enhancement method as CoSICA. The overall framework for the proposed method is illustrated in Figure 3.

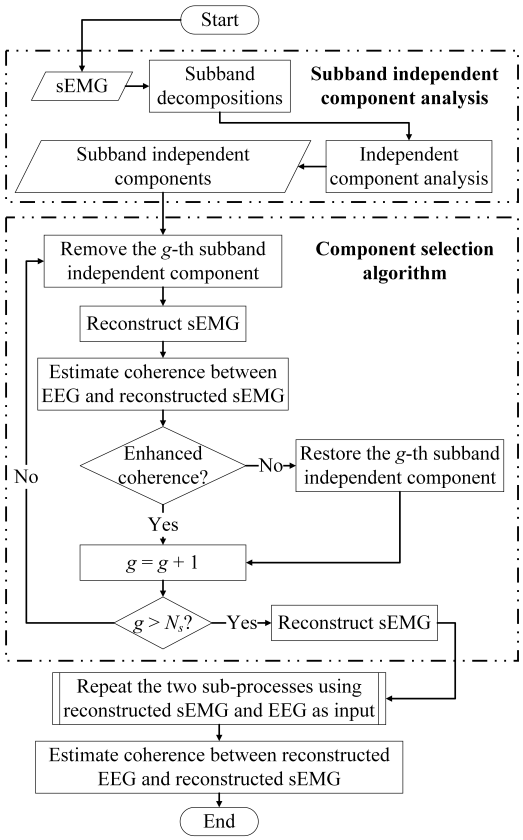

Fig. 3. A block diagram of the proposed CoSICA methodology.

The complexity of the proposed method is equal to the complexity of the component selection algorithm added to the complexity of ICA [52], for which fast implementations exist. The complexity of the component selection algorithm increases linearly in the product of the length of the SICs (subband independent components) and their total number, which is upper-bounded by the product of the number of available sEMG and EEG channels and the number of bands in the employed subband decomposition. In particular, the numerical complexity of the component selection algorithm is $O(MJT)$, where M denotes the number of collected sEMG and EEG channels, J represents the number of wavelet transform or CMFB channels, and T is the duration of the collected signals. This is because the component selection algorithm is performed once for each SIC, and there can be up to MJ SICs, and it involves inversion of the subband decomposition and coherence estimation, the complexity of which is linear in signal duration.

IV. Evaluations Using Synthetic Data

The performance of CoSICA is first evaluated using simulated data under different SNRs. The simulated two-channel EEG signals were generated by the wavelet-based method proposed in [53]. In order to mimic a motor control task, only the component corresponding to the β band (16-32 Hz) was regarded as the cortical excitation signal that was related to the process of interest. To be specific, the simulated two-channel EEG signals were filtered by a Butterworth bandpass filter with a lower cut-off frequency of 16 Hz and a higher cut-off frequency of 32 Hz. The simulated sEMG signal was generated from the sum of the outputs of two linear time-invariant systems, each with a single-channel simulated EEG signal as input. Both systems were modelled as having 1000 paths with attenuation parameters b_i distributed according to a standard Gaussian distribution, and delays D_i following a normal distribution with a mean of 20 ms and standard deviation of 4 ms as described in [54]. We repeated the procedure and generated sEMG signals of two channels.

Three additional components were also added to the simulated sEMG and EEG signals, generated using the sum of sine waves with random amplitudes and phases, distributed uniformly between 0 and 0.3, and 0 and 2π, respectively. Frequencies of these additional components were chosen to be within α, β, and γ bands. Specifically, the components in the α band were the sums of 4 sine waves of frequencies 9 Hz, 10 Hz, 11 Hz, and 12 Hz. Analogously, the components in the β band were the sums of 16 sine waves of frequencies 17 Hz, 18 Hz, ..., 32 Hz, and the components in the γ band were the sums of 28 sine waves of frequencies 37 Hz, 38 Hz, ..., 64 Hz. Since these components are not of interest in the considered motor task, they are regarded as "noise". Finally, pseudorandom Gaussian noise was added to all simulated EEG and sEMG signals. The signal-to-noise ratio (SNR) is calculated by dividing the energy of the noise-free β-band EEG/EMG signal by the sum of the energies of the other components (*i.e.* unrelated α-band, β-band, γ-band components and pseudorandom noise component). Only the power of pseudorandom noise is changed to obtain different SNRs. One sEMG channel was selected as the signal to be denoised, and the other channel was used as the additional input to the CoSICA algorithm to separate independent components from the two-channel sEMG; analogously for the simulated EEG. These simulated data were used to compare the results from the described methodologies with results from standard

CMC estimation, calculated according to (4). Significance levels were calculated according to (5).

The proposed CoSICA method was applied to 200 segments of two-channel sEMG and EEG signals simulated in this manner. Each segment was 250 samples long, and the sampling frequency was 250 Hz. Figure 4 shows the discrete Fourier transform (DFT) magnitude of the simulated EEG/EMG signal of one channel in a single segment under different SNRs. It can be observed from the figure that the spectrum of the noise-free β-band EEG/EMG is confined to the (16-32) Hz range, whereas the spectrum of EEG/EMG with $\mathrm{SNR} \leq -5$ dB is spread out over the whole frequency range.

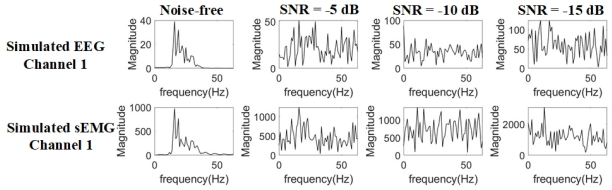

Fig. 4. The DFT magnitude of one channel's simulated EEG/EMG signal under different SNRs.

A comparison of the results from the standard CMC and CoSICA methodologies applied to the simulated signals is shown in Table I. In this experiment, the $Daubechies\ db2$ wavelet was applied, and the number of scales of the SWT was set to 3, hence the subband components $y_{m,3}$ approximately represent the (15.625 - 31.25) Hz, *i.e.* the β band. The number of channels in CMFB was set to 8 which yields subbands' bandwidth of 15.625 Hz, so that the second channel corresponds to the β band. The number of independent components to be estimated in ICA equals the number of input channels (8 for W-ICA and 16 for CMFB-ICA). According to the table, the proposed CoSICA significantly enhances the average β range CMC value. The relative increase in CMC levels exhibits a monotonically increasing trend as the SNR decreases, whereas the overall CMC level increases with the SNR. Furthermore, the highest CMC increase (183.53%) is achieved by CoSICA using SWT for both simulated sEMG and EEG signals at $\mathrm{SNR} = -15$ dB.

V. Evaluations Using Neurophysiological Data

A. Data Acquisition

The studies were conducted in 14 healthy adults (9 female) aged 24-62 years. All were right hand dominant by self-report and none had any history of movement disorders. The experimental arrangements have been reported previously [19] and are illustrated in Figure 5. In brief, the subjects sat at a table and performed a simple grasp task with their right hand, holding a ruler between thumb and index finger, with the wrist and forearm supported to minimise fatigue. Mechanical perturbations were provided from an electromechanical tapper that generated pulses of lateral displacement of the ruler, giving subjects the sensation that their grip on the ruler may be lost. A single trial lasted 5 seconds, with the stimulus delivered 1.1 s after the start of the data collection period. The perturbation lasted for 20 ms with rise time of 5 ms. The stimuli were delivered at pseudorandom intervals between 5.6 s and 8.4 s (mean 7.0 s) to prevent anticipation of the stimulus. Data were collected in blocks of 25 trials (data epochs) with a short rest between blocks to avoid fatigue. Up to 8 blocks of data (200 trials) were collected per subject.

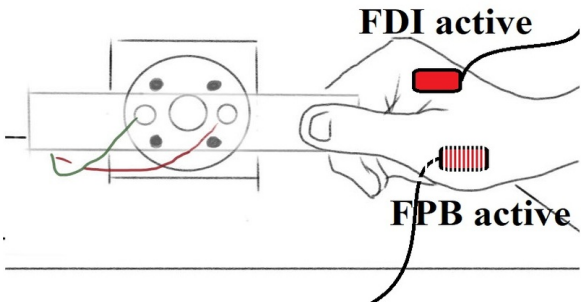

(a) Positions of the tapper, ruler, hand, and sEMG electrodes. The red rectangle indicates the FDI active electrode, whereas the dashed red rectangle represents the FPB active electrode placed on the thenar eminence (on the palmar aspect of the hand). The inactive EMG electrodes were placed over the tendons of the respective muscles (not shown).

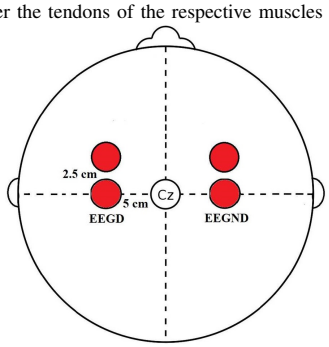

(b) Positions of EEG electrodes. Two bipolar EEG are recorded using four electrodes shown as red circles.

Fig. 5. The collection of EEG and sEMG signals.

The muscle pair, first dorsal interosseous (FDI) and flexor pollicis brevis (FPB), is predominantly activated during this task. EMG was recorded using self-adhesive electrodes in a belly-tendon montage over FDI and FPB of the dominant hand. Two bipolar EEG, *i.e.* EEG from dominant motor cortex (EEGD) and EEG from non-dominant motor cortex (EEGND), were recorded from the scalp overlying the bilateral motor cortex with two electrodes placed 5 cm lateral to the vertex along the interaural line, and the other two electrodes positioned 2.5 cm anterior to them, respectively. EMG and EEG signals were amplified, filtered ($0.5-100$ Hz for EEG; $5-500$ Hz for EMG) and sampled at 1024 Hz. Raw EEG signals were scrutinized off-line by eye and epochs of data containing movement artefacts were rejected from further analysis [19]. Power line noise was removed by a digital notch filter.

B. CMC Enhancement for Neurophysiological Data

In the original neurophysiology study [19], the coherence observed in some subjects was relatively strong, whilst in others it was very weak and remained below the level of significance for that individual throughout the epoch (Table II and Figure 6(a)). For the present study, eight subjects that exhibited different levels of coherence were selected. The FDI signal was used as the sEMG to be de-noised, whilst the FPB

TABLE I
INCREASE OF AVERAGE β RANGE CMC BETWEEN RECONSTRUCTED SEMG AND (RECONSTRUCTED) EEG ACHIEVED BY COSICA FOR SIMULATED DATA UNDER DIFFERENT SNRS.

SNR (dB)	Original	Significance	After CoSICA using SWT for sEMG only		After CoSICA using SWT for sEMG and EEG		After CoSICA using CMFB for sEMG only		After CoSICA using CMFB for sEMG and EEG	
	CMC value	threshold	CMC value	CMC increase (%)	CMC value	CMC increase (%)	CMC value	CMC increase (%)	CMC value	CMC increase (%)
-5	0.3318	0.0149	0.3782	13.98	0.6208	87.10	0.3675	10.76	0.4730	42.56
-10	0.1426	0.0149	0.1834	28.61	0.2913	104.28	0.1678	17.67	0.2436	70.83
-15	0.0340	0.0149	0.0579	70.29	0.0964	183.53	0.0490	44.12	0.0765	125.00

signal was used with FDI for the separation of independent components. Analogously, the EEGD and EEGND signals were used as the EEG to be de-noised and the additional signal to aid blind source separation, respectively. The coherence between EEGD and FDI was estimated in a short-time Fourier domain using a 500 ms-long (512 samples) Hanning window with 250 ms (256 samples) overlaps. The CoSICA was applied to each window of data separately.

The wavelet decomposition of CoSICA, was performed using the *Daubechies db*2 wavelet. Since α $(8-16Hz)$, β $(16-32Hz)$ and γ $(32-64Hz)$ frequency bands have different functions in sensory-motor integration and the sampling rate used was 1024 Hz, in order to approximate this frequency resolution, 6 scales of the wavelet transform were considered. The decision not to separate θ and δ bands is governed by the data acquisition process during which most of the $(0-4)$ Hz EMG content was filtered out, as is common in motor neurophysiology studies, to minimize movement artefact. The number of independent components to be estimated was set to $2\times 7=14$, which is the maximum for the given number of input channels. Alternatively, for the CMFB of CoSICA, the number of channels $J=64$ was selected, corresponding to subband bandwidth of 8 Hz, matching the finest frequency resolution of the wavelet transform; the number of independent components was set to $2\times 64=128$, also the maximum given the number of input channels.

The results of the original CMC patterns for subjects A-H are shown in Figure 6(a), while the baseline results are presented in Table II. According to Figure 6(a) and Table II, subjects A-D exhibit significant β-range CMC during most of the pre-stimulus and post-stimulus periods. Subjects E-H, on the other hand, show only a few brief bursts of significant coherence immediately after the stimulus, and the time-frequency region where CMC is detected is very sparse. Figures 6(e) and 6(f) show CMC enhancement of subjects A-H after CoSICA for both EEG and sEMG, using SWT and CMFB, respectively. The enhancement of CMC levels is evident in all tested cases. After applying CoSICA, in subjects E-H significant coherence appears even where it could not be observed in the post-stimulus period after 2 s. Further, it can be observed that CoSICA using CMFB with $J=64$ achieves the best results.

For a comparative analysis of the effectiveness of CoSICA in CMC enhancement, our evaluations involved three alternative techniques: 1) Wavelet thresholding-based denoising (WTD) [55]: a well-established method for denoising biological signals. Aligned with CoSICA's wavelet decomposition, the *Daubechies db*2 wavelet at six scales was used for the WTD method. 2) Sparse signal representation (SSR): an advanced signal processing approach that has been successfully used in image denoising [56] and speech separation [57]. In this study, the K-SVD algorithm [58], in conjunction with ADMM [59], was employed to derive a dictionary capable of facilitating noise removal and achieving a sparse representation with enhanced accuracy. 3) Sparsity-assisted signal denoising and pattern recognition (SASD-PR) [60]: a recent method capable of concurrently denoising signals while detecting oscillatory patterns of interest. In our investigation, the SASD-PR method was executed with 50 iterations, and the convergence rate parameter was consistently set to 1.

The CMC patterns following the application of the three reference methods and the proposed CoSICA methodology are shown in Figure 6. Corresponding quantitative results, reflecting the averaged β range CMC across all time windows, are detailed in Table III. It can be observed that WTD, SSR, and SASD-PR increased β range CMC levels across much of the experimental trial, but only to a limited extent, with a mean increase less than 20% (Table III). In contrast, CoSICA, particularly when using CMFB, significantly enhances β range coherence levels, achieving an average increase of over 300%.

TABLE II
INDIVIDUAL DATA FOR EEG-SEMG COHERENCE.

Subject	Age	Gender	Average original β range CMC in the pre-stimulus window[a]	Average original β range CMC in the post-stimulus window[b]	Significance threshold[c]
A	39	Female	0.0255	0.0702	0.0166
B	44	Female	0.0268	0.0693	0.0154
C	25	Male	0.0331	0.0902	0.0167
D	26	Female	0.0088 (NS)[d]	0.0224	0.0149
E	32	Male	0.0113 (NS)	0.0064 (NS)	0.0149
F	32	Female	0.0044 (NS)	0.0086 (NS)	0.0179
G	24	Female	0.0069 (NS)	0.0123 (NS)	0.0157
H	36	Male	0.0063 (NS)	0.0172 (NS)	0.0177

[a] The pre-stimulus period was defined as -1.1 to -0.6 s.
[b] The post-stimulus period was defined as 0.4 to 0.9 s.
[c] The significance threshold is individualized for each subject, as it depends on the number of trials of data once artefact-contaminated trails have been removed.
[d] The abbreviation "NS" stands for "non-significant".

Lastly, the impact of some CoSICA parameters on the effectiveness of CMC enhancement is investigated. Taking the averaged β range CMC across all time windows in subject A as an example, Tables IV and V show how the coherence value changes under different levels of wavelet decomposition and different number of CMFB channels, when the preset initial number of sought independent components varies. According to Tables IV and V, when the number of subbands is fixed, the coherence increases with the number of independent components; also, when the number of independent components is fixed, the coherence increases with the number of

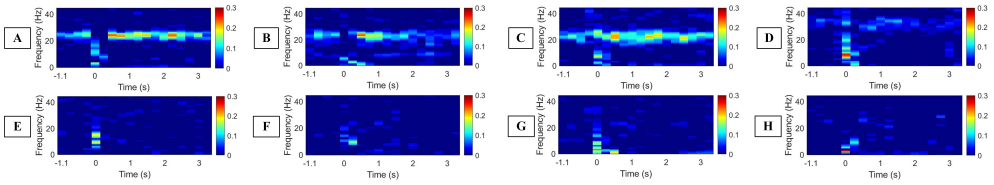

(a) Original CMC.

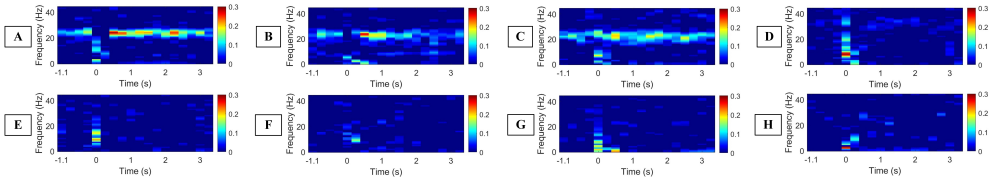

(b) CMC after denoising performed by applying WTD for sEMG and EEG with $db2$ wavelet at 6 scales.

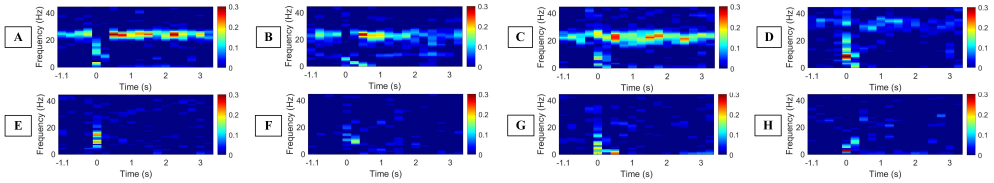

(c) CMC after denoising performed by applying SSR for sEMG and EEG.

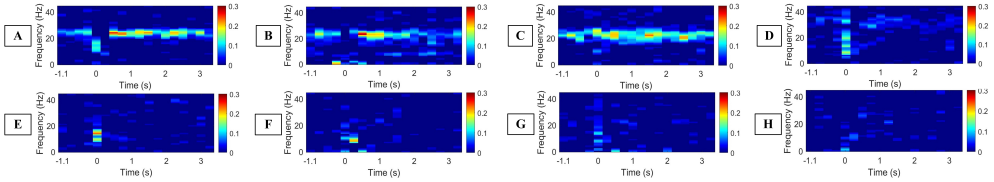

(d) CMC after denoising performed by applying SASD-PR for sEMG and EEG.

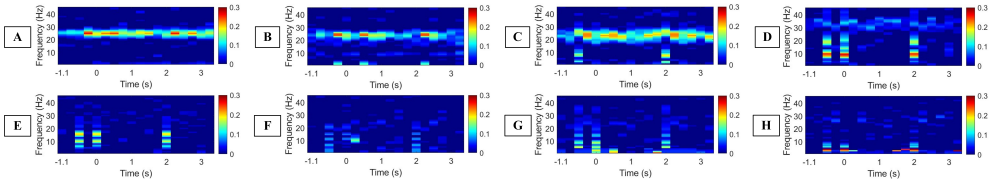

(e) CMC after CoSICA for sEMG and EEG using SWT with $db2$ wavelet at 6 scales.

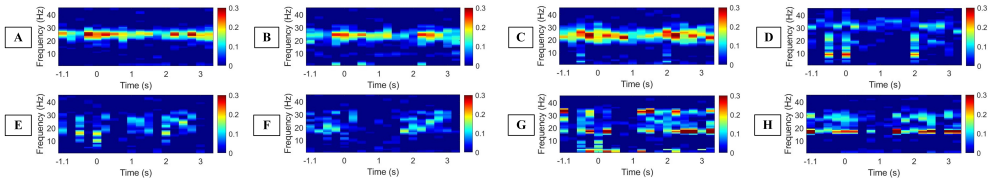

(f) CMC after CoSICA for sEMG and EEG using CMFB with $J = 64$, which yields subbands' bandwidth of 8 Hz.

Fig. 6. CMC spectrograms before and after WTD, SSR, SASD-PR, and CoSICA for sEMG and EEG in subjects A-H. The stimulus is applied at time zero. Note that the colour scale is set such that dark blue represents values falling below the level of significance for that individual, whereas brighter colours show significant coherence.

subbands. Comparing the CoSICA using SWT at 6 or more scales and CMFB with 8 or 16 channels, CoSICA based on the wavelet transform achieves more substantial coherence increase, even when the number of employed independent components in CMFB analysis is higher (*e.g.* CMFB with 16 channels and 24 and 32 independent components). Note that at 1024 Hz sampling, owing to their uniform frequency resolution, CMFBs need at least 32 channels to separate the β band from EEG and sEMG signals, whereas the wavelet transform achieves that already at 6 scales (7 channels). Hence, when the number of CMFB channels increases to 32 or above, the performance improves beyond that achieved by the wavelet transform. It can be further observed that the increase in the number of scales of the wavelet transform to 7 (8 channels) leads to only a marginal increase in the average coherence in the β range, which is not unexpected considering that the additional scale in the wavelet transform only separates the low-frequency θ and δ components and the δ oscillations have been filtered out in the acquisition process to remove movement artefacts [19]. Any further increase in

TABLE III
QUANTITATIVE COMPARISON OF COHERENCE ENHANCEMENT ACROSS WTD, SSR, SASD-PR, AND COSICA.

Methods	Subject A		Subject B		Subject C		Subject D		Subject E		Subject F		Subject G		Subject H		Mean Increase (%)
	Coherence Value	Increase (%)	Coherence Value	Increase (%)	Coherence Value	Increase (%)	Coherence Value	Increase (%)	Coherence Value	Increase (%)	Coherence Value	Increase (%)	Coherence Value	Increase (%)	Coherence Value	Increase (%)	
Original Coherence	0.0455	-	0.0385	-	0.0604	-	0.0164	-	0.0084	-	0.0072	-	0.0082	-	0.0082	-	-
WTD	0.0484	6.37%	0.0415	7.79%	0.0605	0.17%	0.0172	4.88%	0.0098	16.67%	0.0077	6.94%	0.0089	8.54%	0.0091	10.98%	7.79%
SSR	0.0546	20.00%	0.0461	19.74%	0.0723	19.70%	0.0196	19.51%	0.0097	15.48%	0.0086	19.44%	0.0098	19.51%	0.0100	21.95%	19.42%
SASD-PR	0.0455	0.00%	0.0452	17.40%	0.0636	5.30%	0.0176	7.32%	0.0096	14.29%	0.0087	20.83%	0.0094	14.63%	0.0086	4.88%	10.58%
CoSICA-SWT	0.0582	27.91%	0.0517	34.29%	0.0779	28.97%	0.0255	55.49%	0.0149	77.38%	0.0111	54.17%	0.0136	65.85%	0.0113	37.80%	47.73%
CoSICA-CMFB	0.0760	67.03%	0.0741	92.47%	0.1134	87.75%	0.0372	126.83%	0.0371	341.67%	0.0386	436.11%	0.0732	792.68%	0.0736	797.56%	342.76%

the number of scales of the wavelet transform would only provide finer frequency resolution in the δ band, which is not relevant to movement control. An increase in the number of channels of CMFB decompositions, on the other hand, results in uniform improvements of the frequency resolution across all bands, which, as results in Table V demonstrate, leads to progressively more pronounced coherence enhancement. Limits of this trend are illustrated by Figure 7, which shows the dependence of the average enhancement of CMC by means of CoSICA on the number of CMFB channels. In particular, the dots in the figure represent the ratio of CMC after and before CoSICA averaged over β range frequencies and over time, with the time segment containing the stimulus excluded, as it was an outlier dominating the results. The horizontal bars show standard deviations of the coherence ratios across the time segments. We can observe that the effectiveness of CoSICA improves as the number of CMFB channels increases up to 128, which corresponds to 4 Hz frequency resolution across all the bands, however, we observed that the results also vary more considerably along the time axes as the number of channels increases, as reflected in the corresponding standard deviations. It should be noted that any increase in the number of channels is accompanied by a proportionate increase in the computational complexity.

TABLE IV
COHERENCE AFTER APPLYING COSICA FOR SEMG AND EEG USING SWT WITH DIFFERENT LEVELS OF WAVELET DECOMPOSITION AND DIFFERENT NUMBERS OF INDEPENDENT COMPONENTS TO BE ESTIMATED.

Level of wavelet decomposition	Number of independent components	Coherence value	Coherence increase (%)
7	16	0.0584	28.35
	12	0.0577	26.81
	7	0.0574	26.15
6	14	0.0582	27.91
	10	0.0574	26.15
	6	0.0573	25.93
4	10	0.0573	25.93
	7	0.0561	23.30
	4	0.0554	21.76
2	6	0.0536	17.80
	4	0.0529	16.26
	2	0.0512	12.53

VI. DISCUSSION

It is well recognised that CMC is heterogeneous across individuals [18], [61], [62], [63] and that standard coherence methods often fail to detect significant cortex-muscle interactions, even in healthy individuals with normal motor control performing motor tasks under the same experimental conditions [18], [19], [64]. This may relate in part to inter-individual differences in cortical processing of movement-related information [63] and also to methodological issues, including the influence of physiological noise [20]. Motivated by the need to enhance the coherence levels degraded by a considerable amount of noise and interference activities in EEG and sEMG signals, we proposed CoSICA, which relies on either SWT or CMFB for subband decomposition and ICA, along with a component selection algorithm.

Using simulated data, it is shown that the noise severely impairs the ability of traditional CMC measurement to reveal underlying interactions (Table I). After applying the proposed CoSICA, CMC was increased substantially. We further found that using SWT for subband decomposition outperforms using CMFB. Both simulated EMG and EEG were degraded by noise, including WGN and irrelevant α, β and γ components. At the sampling rate of 250 Hz and the wavelet transform at three scales, the SWT subbands match the bands of the synthesised θ/δ, α, β, and γ processes, (0-15.625), (15.62 - 31.25), and (31.25 - 62.5) Hz, respectively, which explains the superior performance of the wavelet transform with the

TABLE V
COHERENCE AFTER APPLYING COSICA FOR SEMG AND EEG USING CMFB WITH DIFFERENT NUMBERS OF CHANNELS AND DIFFERENT NUMBERS OF INDEPENDENT COMPONENTS TO BE ESTIMATED.

Number of CMFB channels	Number of independent components	Coherence value	Coherence increase (%)
64	128	0.0760	67.03
	96	0.0719	58.02
	64	0.0657	44.40
32	64	0.0603	32.53
	48	0.0595	30.77
	32	0.0586	28.79
16	32	0.0569	25.05
	24	0.0564	23.96
	16	0.0525	15.38
8	16	0.0487	7.03
	12	0.0479	5.27
	8	0.0470	3.30

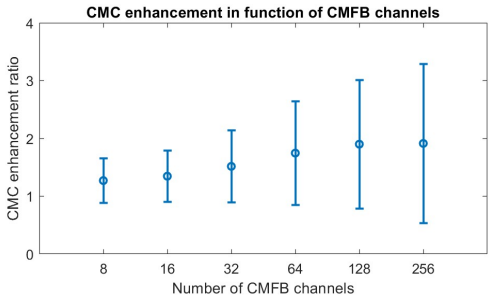

Fig. 7. The effect of the number of CMFB channels on the effectiveness of CoSICA. The dots represent the ratio of CMC after and before CoSICA averaged over β range frequencies and over time segments, whereas the horizontal lines show corresponding standard deviations across the time segments.

simulated data, in which there was known coherence between the EEG and EMG over the whole β band.

We then conducted a comparative analysis to assess the efficacy of CoSICA in detecting communications between the cortex and muscle during a motor task. In the present study, denoising methods, including WTD, SSR, and SASD-PR, did not achieve pronounced enhancements (Figures 6(b), 6(c), and 6(d)). Various other noise reduction methods have been published for electrophysiological signals, but many are not comparable as they were developed for use with high density sEMG [65], [66] or multi-channel signals [67], [68], and additionally are designed to remove specific, non-neurological noise elements such as ECG [65], baseline drift [69], or mains interference [70] from the signals. In contrast, the CoSICA technique aims to filter not only specific noise components but also physiological components unrelated to the considered movement task. Among the compared methods, CoSICA using CMFB with $J = 64$ channels achieved the best performance in increasing CMC levels (Figure 6(f)). For the physiological data, the genuine coherence is likely to involve bands narrower than the entire β band. This is illustrated in [19], and in Figure 6(a) of this paper, in which it is seen that individual subjects tend to show CMC across 8 Hz frequency bands within the β range. Given a sampling frequency of 1024 Hz, CMFB separated the composite signal into 64 subbands, each with a constant bandwidth of 8 Hz. It is therefore not surprising that a method with a matched frequency resolution would perform better with the physiological data.

The present study also investigated the effect of CoSICA parameters on CMC enhancement (Tables IV and V). With the number of subbands fixed, the coherence increases with the number of independent components. The observations suggest that a relatively large number of independent components may facilitate the separation of sources involved in the considered motor task, reflecting the heterogeneity of EEG/EMG signals. Further, with the number of independent components fixed, the coherence increases with the number of subbands. The increased number of subbands in each electrode and finer frequency resolution also facilitates the separation of independent sources. Interestingly, when comparing the CoSICA using SWT at 6 scales (7 channels) and CMFB with 8 or 16 channels, CoSICA with the wavelet decomposition achieves more substantial coherence enhancement, which can be attributed to the fact that at the sampling frequency of 1024 Hz, the SWT at 6 scales separates $(0-8)$ Hz, $(8-16)$ Hz, $(16-32)$ Hz, and $(32-64)$ Hz bands which have distinct functions in sensory-motor integration, by matching their frequency resolution, whereas the frequency resolution of an 8 or 16-channel CMFB is too coarse to achieve their separation. However, when the number of CMFB channels increases to 32 and above, so that at least the β band is extracted from sEEG and EMG signals, CoSICA with CMFB outperforms that with the wavelet transform. The performance further improves as the number of CMFB channels increases, so that the α band is extracted too, and the frequency resolution of signal decomposition across all bands is refined. This trend continues to 128 channels, which at 1024 Hz sampling frequency corresponds to 4 Hz subbands, suggesting that narrower frequency bands might extract additional information. Optimal subband decomposition in CoSICA of neurophysiological signals requires further investigation that would include time-varying filter banks and wavelet packets [48]. Nevertheless, our investigation here indicates that the subband decomposition should at least separate the functional bands of neural oscillations and ideally achieve additional within band decomposition. In this study we only used two EEG channels over sensorimotor cortex. This was a practical choice aimed at limiting the duration of data acquisition and associated costs, but future work could apply this technique to recordings using a larger number of EEG electrodes and therefore a wider cortical representation.

It is noted that in addition to removing noise, the CoSICA method focuses the analysis on the most relevant parts of the signal and removes those parts which are unrelated to the communication between the cortex and muscles, through its component selection algorithm. Along with the considerable improvements in CMC levels demonstrated by the proposed technique in both simulated and neurophysiological data, further improvements could potentially be achieved by exploring different techniques at the data collection stage. Some examples include: 1) improving the spatial resolution of the sensorimotor cortex EEG using a bipolar montage [51]; 2) using single motor unit EMG recordings [3]; 3) maintaining attention on the motor task (dividing attention by simultaneously performing a mental arithmetic task led to reduced levels of coherence) [62]; 4) accounting for the time-lag between cortex and muscle activities [54]; 5) applying a peripheral stimulus relevant to the task [19].

The proposed CoSICA is of relevance as CMC has been increasingly advocated as a potentially inexpensive and useful method to study the mechanism of cerebral cortex's control of muscle activity in healthy ageing [71], and to investigate a functional connection between the cortex and muscles in stroke and sports disorders patients during rehabilitation [72], [73], [74]. Abnormalities of CMC and its modulation have been demonstrated also in patients with dystonia, with the pattern of abnormality differing according to the underlying aetiology [16]. Studies have similarly proposed its potential utility in a variety of neuro-degenerative disorders, such as Parkinson's disease (PD) [75], [74]. For instance, CMC has already been used as a neuro-physiological indicator of functional coupling between the primary motor cortex and peripheral muscles and as an index for PD symptom variation [72], [73], [75], [74]. CMC has also shown utility as a therapeutic indicator in PD patients [75], [74]. Moreover, some authors propose its utility as a biomarker of the rehabilitation potential of the deep brain stimulation (DBS) of the subthalamic nucleus (STN), which is used to normalize pathologically altered oscillations in PD patients [76], [74]. For example, STN-DBS has been shown to increase the amplitude of 10-30 Hz CMC in PD patients, likely due to the improvement of tremor by DBS [76]. Thus, CMC may be associated with the therapeutic effects of DBS and other neuro-modulation technologies. Similar to DBS, the transcranial alternating current stimulation (tACS) can modulate cortical brain activity. Krause *et al.* showed that decreased β band CMC and variability of fast lateral

movements were due to motor cortex tACS at 20 Hz in PD patients [75]. Therefore, CMC can enhance understanding of pathophysiological mechanisms and has potential translational use as a clinical biomarker. However, tools to enhance the detection of CMC, such as the methods proposed here, are needed for these applications to be realised.

Past studies using directional coherence analysis have emphasized that CMC reflects both the cortico-efferent descending signals from motor cortex to muscles, as well as ascending cortico-afferent signals from muscles to motor cortex [73], [77], [74]. Moreover, numerous studies have shown that the factors that may affect CMC include the cortico-muscular coordination, experimental design [78], [79], band frequencies [79], force levels [80], age [71], and difference between healthy controls and patients [75], [74]. In order to overcome these challenges, future studies will need to focus in a greater depth on understanding the relationship between cortical and muscular activities and the applications in rehabilitation field and clinical field in general, requiring greater resources and data acquisition. If CMC is to become a standard of motion decoding, it may eventually help exploit new rehabilitation protocols in a number of major neurologic, neuro-degenerative and even (functional) psychiatric disorders [74].

VII. Conclusion

In this paper, we proposed a denoising method, CoSICA, based on the joint use of SWT/CMFB, ICA, and a component selection algorithm. The components were selected by the algorithm with the purpose of enhancing the coherence between monitored cortex and muscle activities. By using simulated data, the effectiveness of CoSICA was demonstrated under different SNRs. The potential of CoSICA to increase the detection of CMC using physiological data was also evidenced. Finally, we demonstrated potential benefits of this novel technique by comparing its results to those obtained using the WTD, SSR and SASD-PR techniques for noise removal. In the advent of increasing calls for individualised medicine and domiciliary and ambulatory treatment delivery, the proposed method provides a framework for enhancing the detection of CMC especially when there are few EEG and EMG channels, which are of particular importance for minimizing the costs and complexity of data acquisition procedures.

References

[1] Y. Xu *et al.*, "Cortico-muscular coherence enhancement via coherent wavelet enhanced independent component analysis," in *2017 39th Annual International Conference of the IEEE Engineering in Medicine and Biology Society (EMBC)*. IEEE, 2017, pp. 2786–2789.

[2] B. Conway *et al.*, "Synchronization between motor cortex and spinal motoneuronal pool during the performance of a maintained motor task in man," *The Journal of Physiology*, vol. 489, no. 3, pp. 917–924, 1995.

[3] S. Baker, E. Olivier, and R. Lemon, "Coherent oscillations in monkey motor cortex and hand muscle EMG show task-dependent modulation," *The Journal of Physiology*, vol. 501, no. Pt 1, p. 225, 1997.

[4] D. M. Halliday *et al.*, "Using electroencephalography to study functional coupling between cortical activity and electromyograms during voluntary contractions in humans," *Neuroscience Letters*, vol. 241, no. 1, pp. 5–8, 1998.

[5] S. N. Baker, "Oscillatory interactions between sensorimotor cortex and the periphery," *Current Opinion in Neurobiology*, vol. 17, no. 6, pp. 649–655, 2007.

[6] M. Hallett *et al.*, "Evaluation of movement and brain activity," *Clinical Neurophysiology*, vol. 132, no. 10, pp. 2608–2638, 2021.

[7] L. Timmermann *et al.*, "Pathological oscillatory coupling within the human motor system in different tremor syndromes as revealed by magnetoencephalography," *Neurology & Clinical Neurophysiology: NCN*, vol. 2004, pp. 26–26, 2004.

[8] C. S. Everlo *et al.*, "Electrophysiological testing aids the diagnosis of tremor and myoclonus in clinically challenging patients," *Clinical Neurophysiology Practice*, vol. 7, pp. 51–58, 2022.

[9] A.-F. van Rootselaar *et al.*, "Coherence analysis differentiates between cortical myoclonic tremor and essential tremor," *Movement Disorders*, vol. 21, no. 2, pp. 215–222, 2006.

[10] A. G. Munts *et al.*, "Clinical and neurophysiological characterization of myoclonus in complex regional pain syndrome," *Movement Disorders: Official Journal of the Movement Disorder Society*, vol. 23, no. 4, pp. 581–587, 2008.

[11] J. N. Caviness *et al.*, "Analysis of high-frequency electroencephalographic-electromyographic coherence elicited by speech and oral nonspeech tasks in Parkinson's disease," *Journal of Speech, Language, and Hearing Research*, vol. 49, no. 2, pp. 424–438, 2006.

[12] ——, "Corticomuscular coherence is increased in the small postural tremor of Parkinson's disease," *Movement Disorders: Official Journal of the Movement Disorder Society*, vol. 21, no. 4, pp. 492–499, 2006.

[13] M. McKeown *et al.*, "Cortical muscle coupling in Parkinson's disease (PD) bradykinesia," in *Parkinson's Disease and Related Disorders*. Springer, 2006, pp. 31–40.

[14] P. Grosse *et al.*, "Abnormal corticomuscular and intermuscular coupling in high-frequency rhythmic myoclonus," *Brain*, vol. 126, no. 2, pp. 326–342, 2003.

[15] E. M. Foncke *et al.*, "Abnormal low frequency drive in myoclonus-dystonia patients correlates with presence of dystonia," *Movement Disorders: Official Journal of the Movement Disorder Society*, vol. 22, no. 9, pp. 1299–1307, 2007.

[16] V. M. McClelland *et al.*, "Abnormal patterns of corticomuscular and intermuscular coherence in childhood dystonia," *Clinical Neurophysiology*, vol. 131, no. 4, pp. 967–977, 2020.

[17] J. McAuley and J. Rothwell, "Identification of psychogenic, dystonic, and other organic tremors by a coherence entrainment test," *Movement Disorders: Official Journal of the Movement Disorder Society*, vol. 19, no. 3, pp. 253–267, 2004.

[18] S. Salenius and R. Hari, "Synchronous cortical oscillatory activity during motor action," *Current Opinion in Neurobiology*, vol. 13, no. 6, pp. 678–684, 2003.

[19] V. M. McClelland, Z. Cvetkovic, and K. R. Mills, "Modulation of corticomuscular coherence by peripheral stimuli," *Experimental Brain Research*, vol. 219, no. 2, pp. 275–292, 2012.

[20] Z. Guo *et al.*, "Multiscale wavelet transfer entropy with application to corticomuscular coupling analysis," *IEEE Transactions on Biomedical Engineering*, vol. 69, no. 2, pp. 771–782, 2021.

[21] ——, "Structured errors-in-variables modelling for cortico-muscular coherence enhancement," in *ICASSP 2023-2023 IEEE International Conference on Acoustics, Speech and Signal Processing (ICASSP)*. IEEE, 2023, pp. 1–5.

[22] J. V. Basmajian, "Muscles alive. their functions revealed by electromyography," *Academic Medicine*, vol. 37, no. 8, p. 802, 1962.

[23] C. J. De Luca and R. Merletti, "Surface myoelectric signal cross-talk among muscles of the leg," *Electroencephalography and Clinical Neurophysiology*, vol. 69, no. 6, pp. 568–575, 1988.

[24] K. Türker and T. Miles, "Cross-talk from other muscles can contaminate EMG signals in reflex studies of the human leg," *Neuroscience Letters*, vol. 111, no. 1-2, pp. 164–169, 1990.

[25] R. R. Vázquez *et al.*, "Blind source separation, wavelet denoising and discriminant analysis for EEG artefacts and noise cancelling," *Biomedical Signal Processing and Control*, vol. 7, no. 4, pp. 389–400, 2012.

[26] D. Moshou *et al.*, "Wavelets and self-organising maps in electromyogram (EMG) analysis," in *Proceedings of the ESIT*. Citeseer, 2000, pp. 14–15.

[27] A. Phinyomark, C. Limsakul, and P. Phukpattaranont, "An optimal wavelet function based on wavelet denoising for multifunction myoelectric control," in *2009 6th International Conference on Electrical Engineering/Electronics, Computer, Telecommunications and Information Technology*, vol. 2. IEEE, 2009, pp. 1098–1101.

[28] L. Yu, "EEG de-noising based on wavelet transformation," in *2009 3rd International Conference on Bioinformatics and Biomedical Engineering*. IEEE, 2009, pp. 1–4.

[29] R. N. Vigário, "Extraction of ocular artefacts from EEG using independent component analysis," *Electroencephalography and Clinical Neurophysiology*, vol. 103, no. 3, pp. 395–404, 1997.

[30] T.-P. Jung *et al.*, "Removing electroencephalographic artifacts by blind source separation," *Psychophysiology*, vol. 37, no. 2, pp. 163–178, 2000.

[31] R. Vigário *et al.*, "Independent component approach to the analysis of EEG and MEG recordings," *IEEE Transactions on Biomedical Engineering*, vol. 47, no. 5, pp. 589–593, 2000.

[32] H. Nakamura *et al.*, "The application of independent component analysis to the multi-channel surface electromyographic signals for separation of motor unit action potential trains: Part I—measuring techniques," *Journal of Electromyography and Kinesiology*, vol. 14, no. 4, pp. 423–432, 2004.

[33] D. Djuwari, D. K. Kumar, and M. Palaniswami, "Limitations of ICA for artefact removal," in *2005 IEEE Engineering in Medicine and Biology 27th Annual Conference*. IEEE, 2006, pp. 4685–4688.

[34] A. Hyvärinen *et al.*, "Independent component analysis of short-time Fourier transforms for spontaneous EEG/MEG analysis," *Neuroimage*, vol. 49, no. 1, pp. 257–271, 2010.

[35] B. Azzerboni *et al.*, "Neural-ICA and wavelet transform for artifacts removal in surface EMG," in *2004 IEEE International Joint Conference on Neural Networks (IEEE Cat. No. 04CH37541)*, vol. 4. IEEE, 2004, pp. 3223–3228.

[36] X. Ren *et al.*, "Noise reduction based on ICA decomposition and wavelet transform for the extraction of motor unit action potentials," *Journal of Neuroscience Methods*, vol. 158, no. 2, pp. 313–322, 2006.

[37] N. P. Castellanos and V. A. Makarov, "Recovering EEG brain signals: Artifact suppression with wavelet enhanced independent component analysis," *Journal of Neuroscience Methods*, vol. 158, no. 2, pp. 300–312, 2006.

[38] J. Taelman, S. Van Huffel, and A. Spaepen, "Wavelet-independent component analysis to remove electrocardiography contamination in surface electromyography," in *2007 29th Annual International Conference of the IEEE Engineering in Medicine and Biology Society*. IEEE, 2007, pp. 682–685.

[39] G. Inuso *et al.*, "Wavelet-ICA methodology for efficient artifact removal from electroencephalographic recordings," in *2007 International Joint Conference on Neural Networks*. IEEE, 2007, pp. 1524–1529.

[40] N. Mammone, F. La Foresta, and F. C. Morabito, "Automatic artifact rejection from multichannel scalp EEG by wavelet ICA," *IEEE Sensors Journal*, vol. 12, no. 3, pp. 533–542, 2011.

[41] M. Zima *et al.*, "Robust removal of short-duration artifacts in long neonatal EEG recordings using wavelet-enhanced ICA and adaptive combining of tentative reconstructions," *Physiological Measurement*, vol. 33, no. 8, p. N39, 2012.

[42] C. Y. Sai *et al.*, "Automated classification and removal of EEG artifacts with SVM and wavelet-ICA," *IEEE Journal of Biomedical and Health Informatics*, vol. 22, no. 3, pp. 664–670, 2017.

[43] R. D. Koilpillai and P. Vaidyanathan, "Cosine-modulated FIR filter banks satisfying perfect reconstruction," *IEEE Transactions on Signal Processing*, vol. 40, no. 4, pp. 770–783, 1992.

[44] G. Carter, C. Knapp, and A. Nuttall, "Estimation of the magnitude-squared coherence function via overlapped fast Fourier transform processing," *IEEE Transactions on Audio and Electroacoustics*, vol. 21, no. 4, pp. 337–344, 1973.

[45] V. M. McClelland, Z. Cvetkovic, and K. R. Mills, "Rectification of the EMG is an unnecessary and inappropriate step in the calculation of corticomuscular coherence," *Journal of Neuroscience Methods*, vol. 205, no. 1, pp. 190–201, 2012.

[46] Z. Cvetkovic, "On discrete short-time Fourier analysis," *IEEE Transactions on Signal Processing*, vol. 48, no. 9, pp. 2628–2640, 2000.

[47] D. R. Brillinger, *Time series: data analysis and theory*. SIAM, 2001.

[48] M. Vetterli and J. Kovačević, *Wavelets and Subband Coding*. Prentice Hall, 1995.

[49] Z. Cvetkovic and M. Vetterli, "Oversampled filter banks," *IEEE Transactions on Signal Processing*, vol. 46, no. 5, pp. 1245–1255, 1998.

[50] T. Q. Nguyen, "Near-perfect-reconstruction pseudo-QMF banks," *IEEE Transactions on Signal Processing*, vol. 42, no. 1, pp. 65–76, 1994.

[51] S. Graziadio *et al.*, "Developmental tuning and decay in senescence of oscillations linking the corticospinal system," *Journal of Neuroscience*, vol. 30, no. 10, pp. 3663–3674, 2010.

[52] V. Laparra, G. Camps-Valls, and J. Malo, "Iterative gaussianization: from ICA to random rotations," *IEEE Transactions on Neural Networks*, vol. 22, no. 4, pp. 537–549, 2011.

[53] D. A. Bridwell *et al.*, "Spatiospectral decomposition of multi-subject EEG: evaluating blind source separation algorithms on real and realistic simulated data," *Brain Topography*, vol. 31, no. 1, pp. 47–61, 2018.

[54] Y. Xu *et al.*, "Corticomuscular coherence with time lag with application to delay estimation," *IEEE Transactions on Biomedical Engineering*, vol. 64, no. 3, pp. 588–600, 2016.

[55] D. L. Donoho, "De-noising by soft-thresholding," *IEEE Transactions on Information Theory*, vol. 41, no. 3, pp. 613–627, 1995.

[56] M. Elad and M. Aharon, "Image denoising via sparse and redundant representations over learned dictionaries," *IEEE Transactions on Image Processing*, vol. 15, no. 12, pp. 3736–3745, 2006.

[57] T. Xu, W. Wang, and W. Dai, "Sparse coding with adaptive dictionary learning for underdetermined blind speech separation," *Speech Communication*, vol. 55, no. 3, pp. 432–450, 2013.

[58] M. Aharon, M. Elad, and A. Bruckstein, "K-SVD: an algorithm for designing overcomplete dictionaries for sparse representation," *IEEE Transactions on Signal Processing*, vol. 54, no. 11, pp. 4311–4322, 2006.

[59] S. Boyd *et al.*, "Distributed optimization and statistical learning via the alternating direction method of multipliers," *Foundations and Trends® in Machine Learning*, vol. 3, no. 1, pp. 1–122, 2011.

[60] G. Prateek, Y.-E. Ju, and A. Nehorai, "Sparsity-assisted signal denoising and pattern recognition in time-series data," *Circuits, Systems, and Signal Processing*, vol. 41, no. 1, pp. 249–298, 2022.

[61] J. Kilner *et al.*, "Task-dependent modulation of 15-30 Hz coherence between rectified EMGs from human hand and forearm muscles," *The Journal of physiology*, vol. 516, no. 2, pp. 559–570, 1999.

[62] R. Kristeva-Feige *et al.*, "Effects of attention and precision of exerted force on beta range EEG-EMG synchronization during a maintained motor contraction task," *Clinical Neurophysiology*, vol. 113, no. 1, pp. 124–131, 2002.

[63] C. N. Riddle and S. N. Baker, "Manipulation of peripheral neural feedback loops alters human corticomuscular coherence," *The Journal of Physiology*, vol. 566, no. 2, pp. 625–639, 2005.

[64] M. Pohja, S. Salenius, and R. Hari, "Reproducibility of cortex–muscle coherence," *Neuroimage*, vol. 26, no. 3, pp. 764–770, 2005.

[65] J. N. Mak, Y. Hu, and K. D. Luk, "An automated ECG-artifact removal method for trunk muscle surface EMG recordings," *Medical Engineering & Physics*, vol. 32, no. 8, pp. 840–848, 2010.

[66] M. Al Harrach *et al.*, "Denoising of HD-sEMG signals using canonical correlation analysis," *Medical & Biological Engineering & Computing*, vol. 55, pp. 375–388, 2017.

[67] A. de Cheveigné, "Sparse time artifact removal," *Journal of Neuroscience Methods*, vol. 262, pp. 14–20, 2016.

[68] A. de Cheveigné *et al.*, "Multiway canonical correlation analysis of brain data," *Neuroimage*, vol. 186, pp. 728–740, 2019.

[69] A. Fasano and V. Villani, "Baseline wander removal for bioelectrical signals by quadratic variation reduction," *Signal Processing*, vol. 99, pp. 48–57, 2014.

[70] A. de Cheveigné, "Zapline: A simple and effective method to remove power line artifacts," *Neuroimage*, vol. 207, p. 116356, 2020.

[71] D. Kamp *et al.*, "Changes of cortico-muscular coherence: an early marker of healthy aging?" *Age*, vol. 35, no. 1, pp. 49–58, 2013.

[72] R. Hari and S. Salenius, "Rhythmical corticomotor communication," *Neuroreport*, vol. 10, no. 2, pp. R1–10, 1999.

[73] B. Hellwig *et al.*, "Tremor-correlated cortical activity detected by electroencephalography," *Clinical Neurophysiology*, vol. 111, no. 5, pp. 806–809, 2000.

[74] J. Liu, Y. Sheng, and H. Liu, "Corticomuscular coherence and its applications: A review," *Frontiers in Human Neuroscience*, vol. 13, p. 100, 2019.

[75] V. Krause *et al.*, "Cortico-muscular coupling and motor performance are modulated by 20 hz transcranial alternating current stimulation (tacs) in parkinson's disease," *Frontiers in Human Neuroscience*, vol. 7, p. 928, 2014.

[76] H. Park *et al.*, "Cortico-muscular coherence increases with tremor improvement after deep brain stimulation in parkinson's disease," *Neuroreport*, vol. 20, no. 16, pp. 1444–1449, 2009.

[77] K. Airaksinen *et al.*, "Cortico-muscular coherence parallels coherence of postural tremor and meg during static muscle contraction," *Neuroscience Letters*, vol. 602, pp. 22–26, 2015.

[78] K. von Carlowitz-Ghori *et al.*, "Corticomuscular coherence in acute and chronic stroke," *Clinical Neurophysiology*, vol. 125, no. 6, pp. 1182–1191, 2014.

[79] H. Schulz *et al.*, "Now i am ready—now i am not: the influence of pre-tms oscillations and corticomuscular coherence on motor-evoked potentials," *Cerebral Cortex*, vol. 24, no. 7, pp. 1708–1719, 2014.

[80] F. Dal Maso *et al.*, "Effect of training status on beta-range corticomuscular coherence in agonist vs. antagonist muscles during isometric knee contractions," *Experimental Brain Research*, vol. 235, no. 10, pp. 3023–3031, 2017.